Supplementary Information (SI) for Inorganic Chemistry Frontiers.

A dual-purpose copper(I) coordination polymer for the construction of self-driven photoinduced C-H arylation systems

Contents

1. General Method

1.1 Materials

1,2,4,5-tetra(2H-tetrazole-5-yl)-benzene) (H_4TTB) was synthesized according to a modified procedure from the literature.[1] Copper(I) cyanide (CuCN, AR) was obtained from Sinopharm Chemical Reagent Co., Ltd. (Shanghai, China). Benzothiazole (**3**, 98 %) was provided by Saen Chemical Technology (Shanghai) Co., Ltd. (Shanghai, China). 4-Iodotoluene (**4a**, 98 %), 3-Iodotoluene (**4b**, 98 %), 2-Iodotoluene (**4c**, 98 %), Iodobenzene (**4d**, 98 %), 1-Chloro-4-iodobenzene (**4e**, 98 %), 2-Iodonaphthalene (**4f**, 98 %), m-iodobenzotrifluoride (**4g**, 98 %), 4-Iodobenzotrifluoride (**4h**, 98 %), lithium tert-butoxide (**LiO*t*Bu**, 99 %), and N, N-Dimethylglycine (**$Me_2NCH_2CO_2H$**, 98 %) were purchased from Anhui ZeSheng Technology Co., Ltd. (Anhui, China). All reagents and solvents were commercially available and used as received without further purification.

1.2 Characterization

Powder X-ray diffraction (PXRD) was executed with the Bruker D8 Advance X-ray diffractometer with Cu $K\alpha_1$. X-ray photoelectron spectroscopy (XPS) spectra were measured by a ThermoFisher Scientific K-Alpha X-ray photoelectron spectroscopy with Al-Kα X-ray source. The thermogravimetric analysis (TGA) was conducted by Netzsch STA 449C thermal analyzer in the air. The morphology and elemental analysis of the samples were obtained by scanning electron microscopy (SEM) (Zeiss MERLIN Compact instrument). Fourier Transform Infrared (FTIR) spectra of all the samples were recorded using a Bruker-ALPHA spectrophotometer with KBr pellets in 400-4000 cm^{-1} region. UV-vis absorption spectra were obtained on a PerkinElmer Lambda 950 spectrophotometer. The Zeta potential of the powder sample film was measured using the Malvern Zetasizer Nano ZS nanoparticle size and Zeta potential analyzer (DLS). Photocurrent measurements and electrochemical impedance spectroscopy (EIS) measurements were performed via the CHI660E electrochemical workstation (Shanghai Chenhua Apparatus) using a conventional three-electrode cell (saturated silver electrode as the reference electrode, Pt plate as the auxiliary electrode), and

Na_2SO_4 solution (0.2 mol L^{-1}) was employed as the electrolyte. The surface roughness images of the films were measured by atomic force microscopy (AFM), and the surface potential of the sample films was carried out by the Kelvin probe force microscopy (KPFM) mode on the Bruker Dimension Icon. The short circuit current (I_{sc}) was tested by a SR570 low-noise current amplifier (Stanford Research System) and the output voltage (V_{oc}) was tested by a high voltage test system for nanogenerator with BIV-26A (Keithley a Tektronix Company with 2657A high power system sourceMeter). The device operating parameters of 5 Hz frequency, 3.5 N load, and 3 cm separation distance were employed for all TEGs, unless specified.

2. Syntheses

Synthesis of $[Cu^{II}(H_2O)_5][Cu^{I}_3(CN)_5]\cdot H_2O$ (1): H_4TTB (0.017 g, 0.05 mmol) and CuCN (0.018 g, 0.2 mmol) were poured into a 15 mL glass vial containing the mixed solvent of 4 mL EtOH and 4 mL DMF, which was sonicated for 30 minutes and then heated at 80°C for 3 days. Upon cooling, blue crystals were collected with a yield of 35% (based on Cu) after washing twice with distilled water and drying under vacuum. Anal. Calcd for $C_{10}H_{24}Cu_8N_{10}O_{12}$: C, 12.20%; H, 2.46%; N, 14.22%. Found: C, 12.15%; H, 2.43%; N, 14.17%. IR (KBr, cm^{-1}): 3406(w), 2803(vw), 2713(vw), 2363(vw), 1631(s), 1382(w), 1349(m), 1129(m), 775 (vw), 619 (vw), 443 (vw).

Synthesis of $(HEDA)[Cu^{I}_4(TTB)(EDA)_2(CN)]$ (Cu^{I}-CP, 2): There are two routes to synthesize **2**. *The first method*: A mixture of H_4TTB (0.017 g, 0.05 mmol), CuCN (0.018 g, 0.2 mmol), EtOH (2 mL), DMF (2 mL), $NH_3\cdot H_2O$ (2 mL), and ethylenediamine (EDA, 2 mL) was placed in a 25 mL Teflon-lined stainless steel autoclave and vigorously stirred for 1 h. The container was sealed and kept at 160°C for 3 days. After cooling to room temperature, light yellow crystals were obtained by centrifugation with a yield of 46% (based on Cu) after washing for three times with EtOH and drying under vacuum. *The second method*: 4 mL ammonia and 4 mL ethylenediamine were added into the glass vial contained **1** along with its mother liquor, which was kept at 80°C for 2 days to obtain light yellow crystals with a yield of 50% (based on Cu). Anal. Calcd for $C_{17}H_{27}Cu_4N_{23}$: C, 25.28%; H, 3.37%; N, 39.88%. Found: C, 25.22%; H, 3.34%; N, 39.80%. IR (KBr, cm^{-1}): 3268 (vw), 2943 (vw), 2867 (vw), 2109 (m), 1653 (w), 1588 (m), 1415 (s), 1362 (m), 1139 (w), 1014 (s), 923 (m), 762 (w), 589 (s).

Assemble of TEGs based on 1 and 2: In a 50 mL round-bottom flask, PVDF (3.75 g), DMAC (*N*,*N*-dimethylacetamide, 8.5 g), and acetone (12.75 g) were stirred at 60°C for 30 minutes. The mixed solution was then cooled naturally to achieve uniform dissolution. Subsequently, the homogeneous solution was spin-coated onto Kapton (Polyimide) film to produce PVDF membrane, which was further adhered to the adhesive side of a Cu tape to fabricate a negative electrode.

After grinding crystals **1** or **2** into fine powders, they were uniformly fixed onto the adhesive side of a Cu tape, with excess powder being blown away using an air gun.

Finally, copper wires were firmly attached onto the other side of each copper tape to ensure good electrical conductivity. Spin-coated PVDF film and **1** or **2** were used as the negative and positive friction materials, respectively. They were combined to fabricate **1**/**2**-TEG devices, working in the vertical contact-separation mode with an effective contact area of 5×5 cm^2.

3. Procedure for the light-induced copper-catalyzed C-H arylation reaction using a 2-TEG device.

The mixture solution of benzothiazole (**3**, 0.5 mmol), iodoarene (**4a**-**h**, 2.5 mmol), catalyst (CuI/**1**/**2**, 15 mol %), $Me_2NCH_2CO_2H$ (30 mol %), Li*O*t*Bu (1.5 mmol), and Et_2O (3 mL) under a N_2 atmosphere was sealed tightly and stirred under irradiation of 14 blue LEDs (1 W) driven by the **2**-TEG device. The reaction temperature was maintained at 23-25°C. After approximately 12 hours, the reaction mixture was cooled, filtrated, washed with Et_2O, and extracted with ethyl acetate and water. The organic phase was separated and concentrated under reduced pressure. The residue was purified by column chromatography on silica gel to obtain pure product **5a**-**h**.

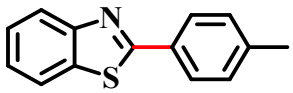

5a

2-(p-Tolyl)benzo[*d*]thiazole: The product is obtained as colorless solid (isolated yield: 90 %). This compound had been reported.[2] ^{1}H NMR (400 MHz, $CDCl_3$) δ: 8.06 (d, J = 8.0 Hz, 1H), 7.98 (d, *J* = 8.0 Hz, 2H), 7.89 (d, *J* = 8.0 Hz, 1H), 7.50-7.45 (m, 1H), 7.39-7.34 (m, 1H), 7.29 (d, *J* =8.0 Hz, 2H), 2.42 (s, 3H).

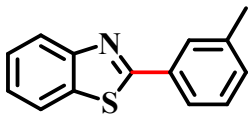

5b

2-(m-Tolyl)benzo[*d*]thiazole: The product is obtained as colorless solid (isolated yield: 88 %), This compound had been reported.[3] ^{1}H NMR (400 MHz, $CDCl_3$) δ: 8.08 (d, *J* = 8.0 Hz, 1H), 7.97-7.86 (m, 3H), 7.53-7.46 (m, 1H), 7.41-7.35 (m, 2H), 7.34-7.29 (m, 1H), 2.46 (s, 3H).

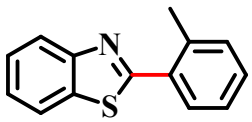

5c

2-(o-Tolyl)benzo[*d*]thiazole: The product is obtained as colorless solid (isolated yield: 89 %). This compound had been reported.[2] ^{1}H NMR (400 MHz, $CDCl_3$) δ: 8.10 (d, *J* = 8.0 Hz, 1H), 7.94 (d, *J* = 8.0 Hz, 1H), 7.76 (d, *J* = 8.0 Hz, 1H), 7.56-7.48 (m, 2H), 7.46-7.31 (m, 3H).

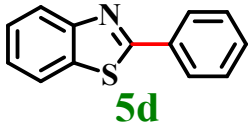

5d

2-Phenylbenzo[*d*]thiazole: The product is obtained as colorless solid (isolated yield: 81 %), This compound had been reported.[3] ^{1}H NMR (400 MHz, $CDCl_3$) δ: 8.12-8.05 (m, 3H), 7.91 (d, *J*=8.0 Hz, 1H), 7.53-7.44 (m, 4H).

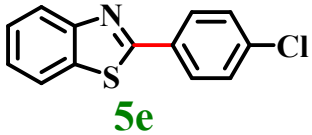

5e

2-(4-Chlorophenyl)benzo[*d*]thiazole: The product is obtained as colorless solid (isolated yield: 75 %), This compound had been reported.[3] ^{1}H NMR (400 MHz, $CDCl_3$) δ: 8.09-8.01 (m, 3H), 7.90 (d, *J* = 8.0 Hz, 1H), 7.52-7.45 (m, 3H), 7.42-7.38 (m, 1H).

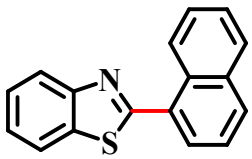

5f

2-(2-naphthyl)benzo[*d*]thiazole: The product is obtained as colorless solid (isolated yield: 79 %), This compound had been reported.[2] ^{1}H NMR (400 MHz, $CDCl_3$) δ: 8.92 (d, *J* = 8.0 Hz, 1H), 8.19 (d, *J* = 8.0 Hz, 1H), 8.03-7.89 (m, 4H), 7.65-7.53 (m, 4H), 7.44 (t, *J* = 8.0, 1H).

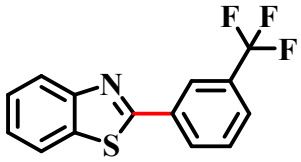

5g

2-[3-(Trifluoromethyl)phenyl]benzo[*d*]thiazole: The product is obtained as colorless solid (isolated yield: 73 %), This compound had been reported.[3] ^{1}H NMR (400 MHz, $CDCl_3$) δ: 8.38 (s, 1H), 8.24 (d, J = 8.0 Hz, 1H), 8.10 (d, J = 8.0 Hz, 1H), 7.92 (d, J = 8.0 Hz, 1H), 7.74 (d, J = 8.0 Hz, 1H), 7.61 (t, J = 8.0 Hz, 1H), 7.52 (t, J = 8.0 Hz, 1H), 7.42 (t, J = 8.0 Hz, 1H).

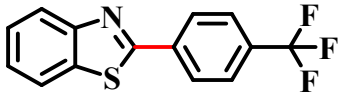

5h

2-[4-(Trifluoromethyl)phenyl]benzo[d]thiazole: The product is obtained as colorless solid (isolated yield: 71 %), This compound had been reported.[3] ^{1}H NMR (400 MHz, $CDCl_3$) δ: 8.22 (d, J = 8.0 Hz, 2H), 8.11 (d, J = 8.0 Hz, 1H), 7.94 (d, J = 8.0 Hz, 1H), 7.76 (d, J = 8.0 Hz, 2H), 7.53 (t, J = 8.0 Hz, 1H), 7.43 (t, J = 8.0 Hz, 1H).

4. Crystal Data Collection and Refinement.

The data of the **1** and **2** was collected on a Bruker D8 Venture using Mo Kα radiation (λ =0.71073) at temperature, respectively. SADABS program was applied to execute the absorption corrections. The structures were solved by direct ways using APEX 3 and refined by full-matrix least-squares on F^2 with the SHELXL.[4,5] All hydrogen atoms expect for H_2O molecule were placed at geometrically calculated positions, and refined by riding. The number of solvent molecules was obtained by element analyses and TGA. The crystal data of **1** and **2** are summarized in **Table S1**and **S2**. **1** and **2** had been deposited at the Cambridge Crystallographic Data Centre with CCDC reference number 2379808 and 2379809, respectively.

Table S1. Crystallographic data and structure refinement details for complexes **1** and **2**.[a, b]

Complex	**1**	**2**
Formula	$C_5H_{12}Cu_4N_5O_6$	$C_{17}H_{27}Cu_4N_{23}$
fw	492.36	807.77
T/K	273.15	293(2)
λ (Mo K), Å	0.71073	0.71073
Crystal system	orthorhombic	monoclinic
Space group	$P2_12_12_1$	$P2_1/n$
a (Å)	7.8686(3)	10.755(2)
b (Å)	10.4759(4)	16.724(3)
c (Å)	18.8777(7)	16.265(3)
β (°)	90	101.41(3)
V (Å3)	1556.10(10)	2867.9(10)
Z	4	4
D_{calcd}.(g·cm^{-3})	2.102	1.871
Reflections collected /unique	32257/6216	29632/5320
abs coeff/mm^{-1}	5.418	2.982
F(000)	964.0	1624.0
2θ (º)	4.316-67.498	3.53-50.996
GOF	1.044	1.141
R_1(I>2sigma(I))[a]	0.0353	0.0860
wR_2(I>2sigma(I))[b]	0.0964	0.2214

[a] $R_1 = \sum||F_o|-|F_c||/\sum|F_o|$. [b] $wR_2 = [\sum w(F_o^2 - F_c^2)^2/\sum w(F_o^2)^2]^{1/2}$.

Table S2. Selected Bond Lengths (Å) and Bond Angles (deg) for **1** and **2**.

1			
Cu1-N1	1.990 (4)	Cu1-N2	2.002 (4)
Cu1-N3[1]	2.105 (5)	Cu1-C1[2]	2.042 (4)
Cu2-N5[3]	2.059 (4)	Cu2-C2	1.932 (4)
Cu2-C3	2.004 (4)	Cu2-C4	1.995 (5)
Cu3-N3[4]	2.025 (4)	Cu3-N4	1.935 (5)
Cu3-C1[5]	2.249 (4)	Cu3-C5	1.910 (4)
N1-Cu1-N2	115.72 (16)	N1-Cu1-N3[1]	108.17 (18)
N1-Cu1-C1[2]	108.52 (17)	N2-Cu1-N3[1]	98.82 (17)
N2-Cu1-C1[2]	111.04 (17)	C1[2]-Cu1-N3[1]	114.46 (19)
C2-Cu2-N5[3]	105.14 (17)	C2-Cu2-C3	121.50 (17)
C2-Cu2-C4	115.6 (2)	C3-Cu2-N5[3]	112.96 (18)
C4-Cu2-N5[3]	99.6 (2)	C4-Cu2-C3	100.16 (18)
N3[4]-Cu3-C1[5]	103.42 (17)	N4-Cu3-N3[4]	106.5 (2)
N4-Cu3-C1[5]	99.21 (18)	C5-Cu3-N3[4]	107.20 (19)
C5-Cu3-N4	124.9 (2)	C5-Cu3-C1[5]	113.51 (16)
O2-Cu4-O1	98.1 (2)	O2-Cu4-O3	88.4 (3)
O2-Cu4-O4	166.5 (3)	O2-Cu4-O5	90.2 (3)
O3-Cu4-O1	98.8 (2)	O4-Cu4-O1	95.3 (3)
O4-Cu4-O3	88.3 (2)	O4-Cu4-O5	89.8 (3)
O5-Cu4-O1	95.46 (19)	O5-Cu4-O3	165.8 (2)

Symmetry codes for **1**: [1]-1/2+X, 1/2-Y, 1-Z; [2]1/2+X, -1/2-Y, 1-Z; [3]1-X, -1/2+Y, 1/2-Z; [4]-1+X, +Y, +Z; [5]+X, 1+Y, +Z.

2			
Cu1-N2	2.124 (6)	Cu1-N8[1]	2.079 (7)
Cu1-N9[1]	2.038 (6)	Cu1-N21	1.878 (8)
Cu2-N1	2.048 (6)	Cu2-N10[1]	2.093 (6)
Cu2-N16	2.064 (7)	Cu2-C15	1.891 (8)
Cu3-N4	1.986 (7)	Cu3-N11[2]	2.109 (6)
Cu3-N15[3]	2.067 (7)	Cu3-N17	2.054 (12)
Cu4-N3[4]	2.097 (6)	Cu4-N7[5]	2.042 (7)
Cu4-N12	2.001 (7)	Cu4-N19	2.099 (10)
N8[1]-Cu1-N2	97.3 (3)	N9[1]-Cu1-N2	98.4 (3)
N9[1]-Cu1-N8[1]	92.4 (3)	N2[1]-Cu1-N2	111.3 (3)
N21-Cu1-N8[1]	126.5 (3)	N21-Cu1-N9[1]	124.7 (3)
N1-Cu2-N10[1]	98.9 (2)	N1-Cu2-N16	91.2 (3)
N16-Cu2-N10[1]	99.0 (3)	C15-Cu2-N1	119.7 (3)
C15-Cu2-N10[1]	120.1 (3)	C15-Cu2-N16	121.9 (3)
N4-Cu3-N11[2]	107.1 (2)	N4-Cu3-N15[3]	121.4 (3)
N4-Cu3-N17	115.9 (4)	N15[3]-Cu3-N11[2]	96.3 (3)
N17-Cu3-N11[2]	103.0 (4)	N17-Cu3-N15[3]	109.6 (4)
N3[4]-Cu4-N19	112.0 (4)	N7[5]-Cu4-N3[4]	96.0 (3)
N7[5]-Cu4-N19	103.0 (4)	N12-Cu4-N3[4]	107.2 (3)
N12-Cu4-N7[5]	125.8 (3)	N12-Cu4-N19	111.7 (3)

Symmetry codes for **2**: [1]1/2+X, 3/2-Y, -1/2+Z; [2]1+X, +Y, +Z; [3]1/2+X, 3/2-Y, 1/2+Z; [4]-1+X, +Y, +Z; [5]-1/2+X, 3/2-Y, -1/2+Z.

5. Additional characterizations for 1 and 2.

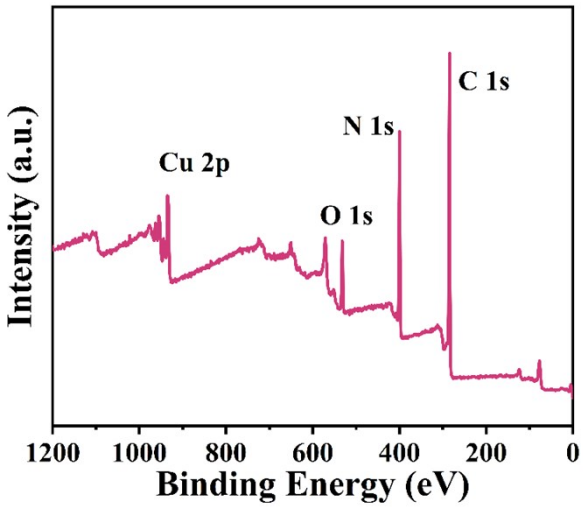

Figure S1. XPS spectrum of **1**.

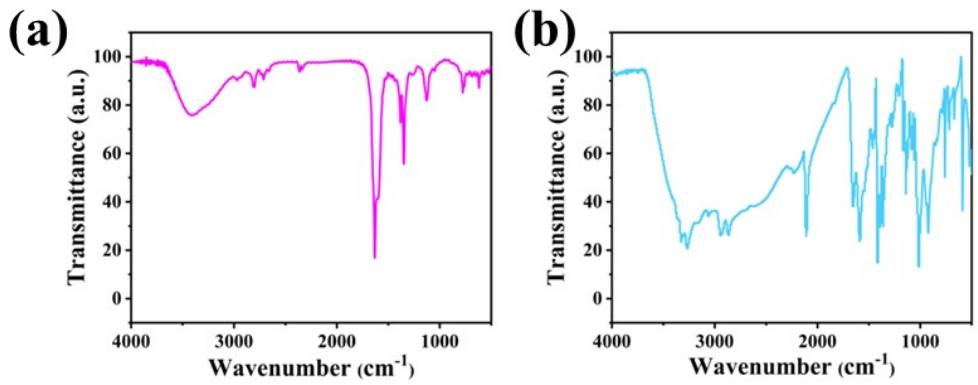

Figure S2. The Fourier-transform infrared (FT-IR) spectra of (a) **1** and (b) **2**.

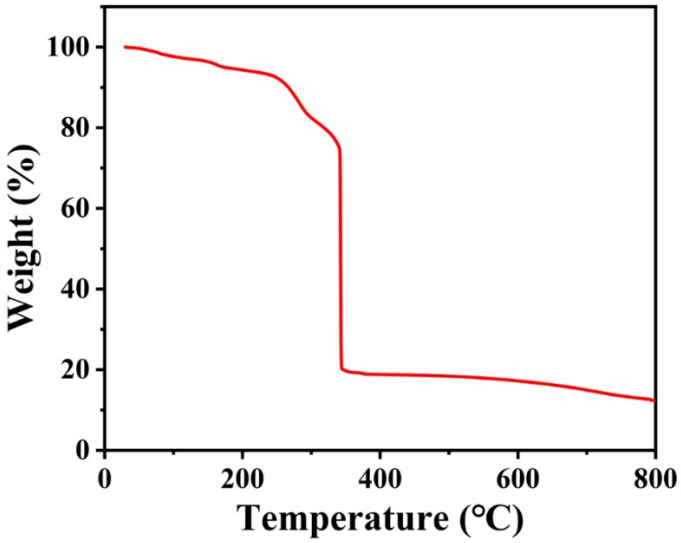

Figure S3. The TG curve of **2**.

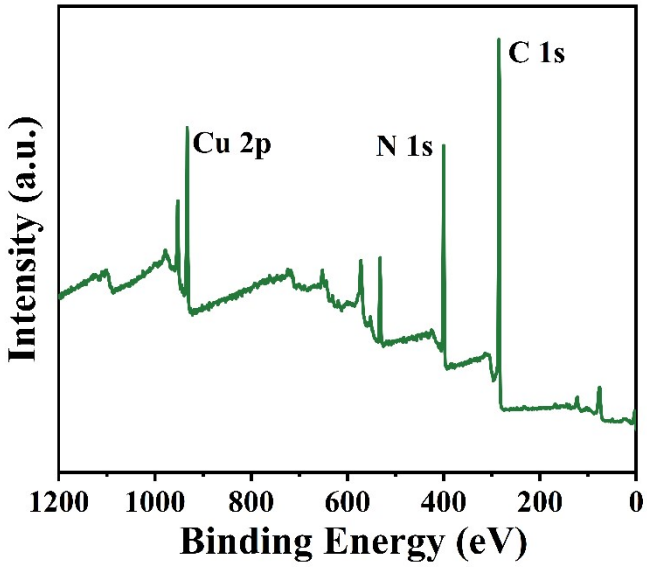

Figure S4. XPS spectrum of **2**.

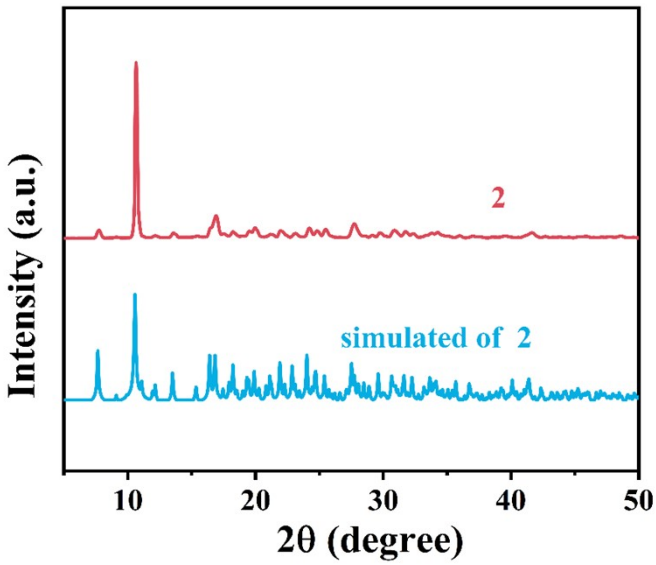

Figure S5. PXRD patterns of **2**.

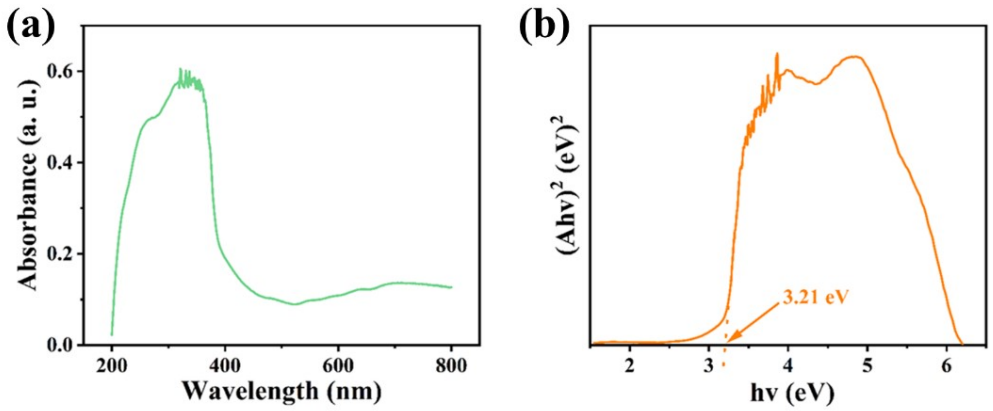

Figure S6. (a) UV-vis of **1**. (b) Tauc plot for **1**.

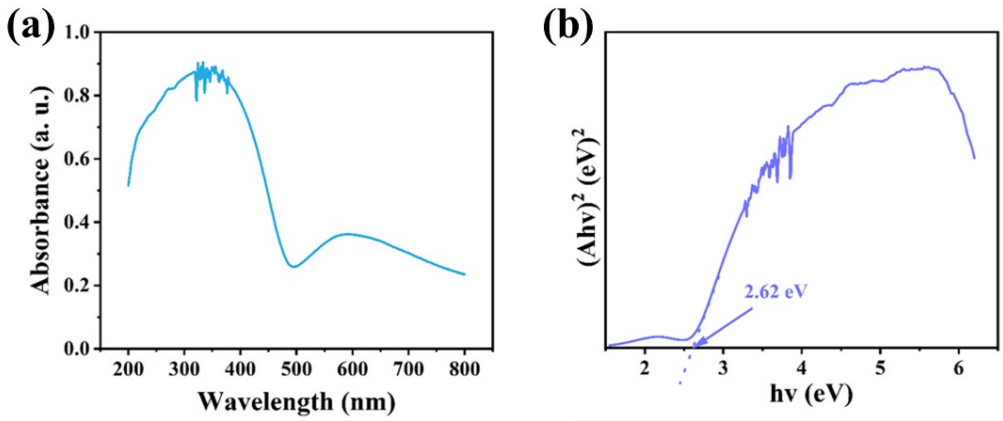

Figure S7. (a) UV-vis of **2**. (b) Tauc plot for **2**.

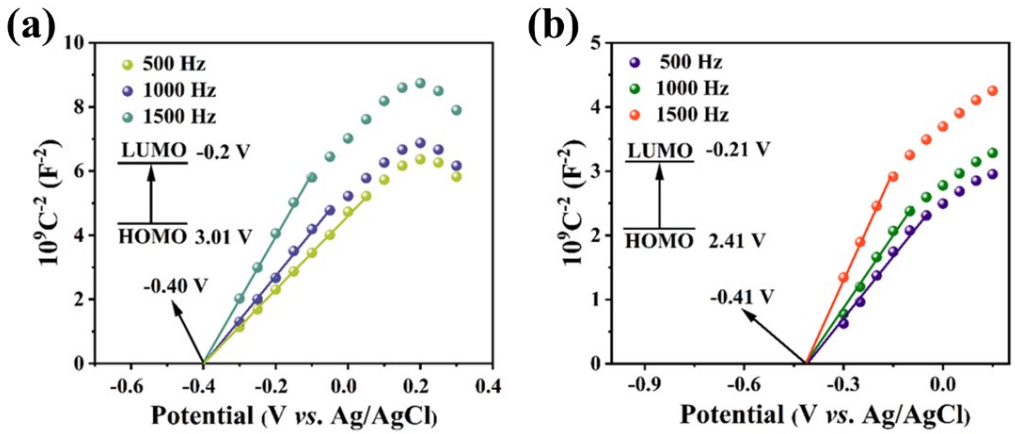

Figure S8. Mott-Schottky plots of (a) **1** and (b) **2**.

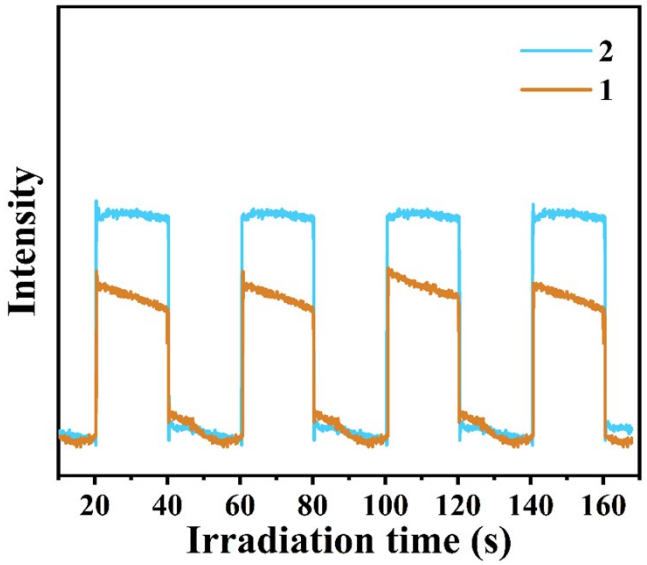

Figure S9. The photocurrent response for **1** and **2**.

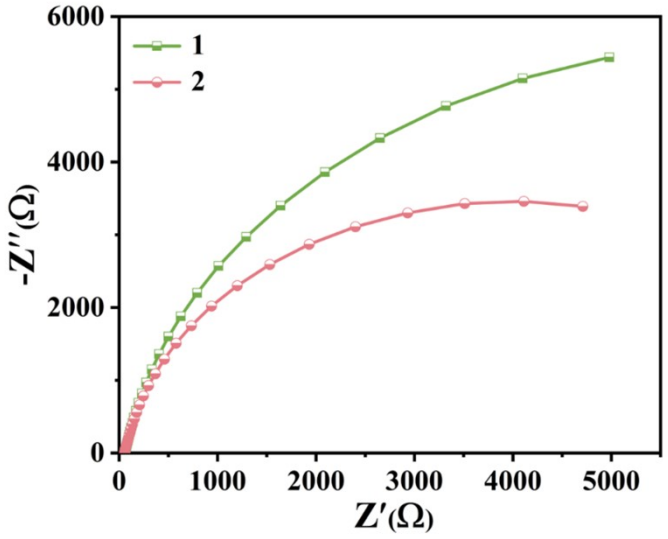

Figure S10. EIS for **1** and **2**.

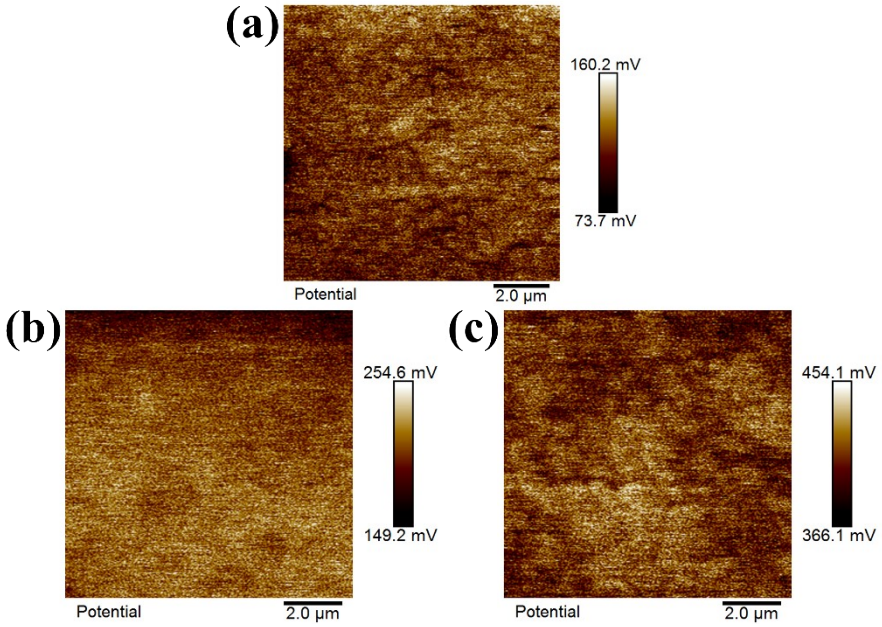

Figure S11. The KPFM images of (a) **1**, (b) H_4TTB and (c) **2**.

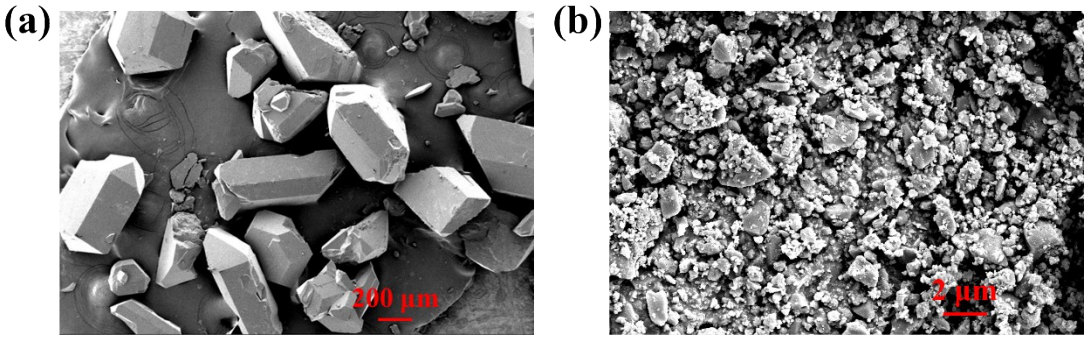

Figure S12. SEM images of **2** (a) before and (b) after grinding.

Table S3. Comparison of our devices with other CP/MOF-based devices reported in literature.

No.	Triboelectric Material	Mode of Operation	Size (cm^2)	I_{sc} ($\mu A/cm^2$)	Power Density (mW/m^2)	Application Type	Ref.
1	UIO-66@PVDF/PVDF	Contact-separation	5 X 5	2	1220	Metal corrosion protection	6
2	ZIF-7/ethyl cellulose		2.5 X 2.5	0.18	7.84	Driving low-power electronic devices	7
3	ZIF-8/Kapton		2.5 X 2.5	1.12	392	Self-powered sensors	8
4	ZIF-67/PET		10 X 10	0.47	593	Gait Monitoring	9
5	Mo-MOF/Kapton		2 X 3	0.08	43.3	Sports or healthcare Monitoring	10
6	Cd-MOF/PVDF		5 X 5	2.21	2451	Driving low-power electronic devices	11
7	NH2-MIL-101(Fe,Cu)@CNF /FEP		4 X 4	0.87	203	/	12
8	NF-MOF@SF/PDMS (ANS-TENG)		2 X 2.5	2.3	2360	Energy Harvester	13
9	CD-MOF/ Teflon		2 X 2	0.3	36.5	Energy Harvester	14
10	Co-MOF/PVDF		5 X 5	3.22	2629.7	Metal corrosion protection	15
11	**2/PVDF**		**5 X 5**	**3.23**	**3120**	**Self-powered photocatalytic system**	**This work**

6. Additional characterizations of 1-TEG and 2-TEG

The TEG generates electrons through the coupling of electrostatic contact electrification and electrostatic induction. In the absence of mechanical force, there is no current output in the external circuit (Figure 3b(i)). When external force is applied, the two electrodes of the TEG device come into contact, and excited-state electrons from the composite film are injected into the PVDF layer, resulting in positive and negative charges on the surfaces of the composite film and PVDF, respectively (Figure 3b(ii)). As the electrodes separate, the potential difference caused by the electrostatic induction effect drives electrons to flow back to the copper layer through the external circuit to balance the local electric field. At this point, the generated charges gradually neutralize (Figure 3b(iii)), and there is no current in the external circuit when the charges reach equilibrium (Figure 3b(iv)). When the two triboelectric electrodes come into contact again, a reverse potential difference is established, causing electrons to flow from the PVDF electrode to the composite film electrode (Figure 3b(v)). Therefore, during the process of contact and separation, under the influence of external force, the TEG continuously generates alternating electrical signals.

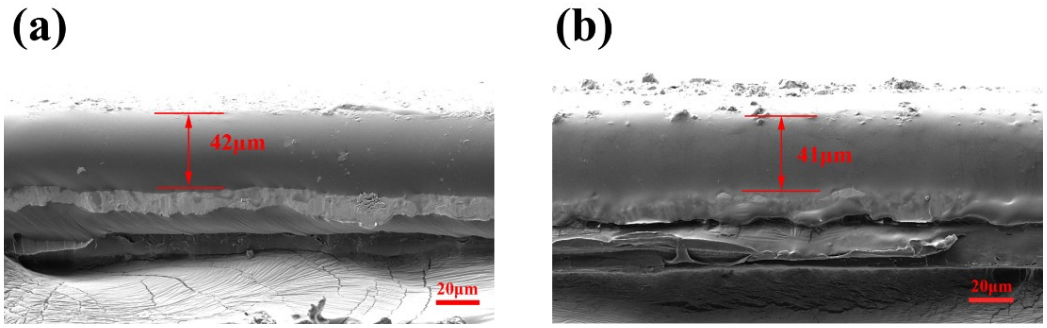

Figure S13. Cross-sectional SEM images of the powder samples (a) **1** and (b) **2** on the Cu layer.

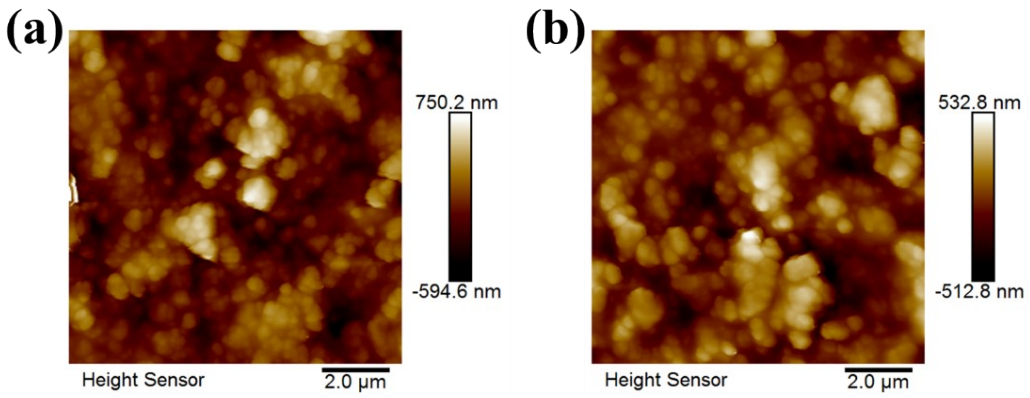

Figure S14. The AFM images of the powder samples (a) **1** and (b) **2** on the Cu layer.

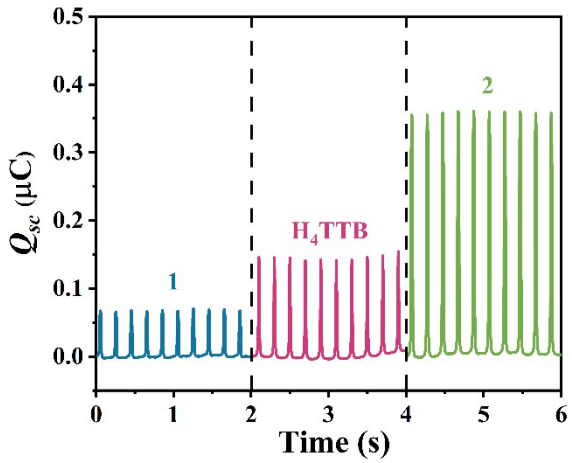

Figure S15. Q_{sc} of the **1**-TEG, H_4TTB-TEG, and **2**-TEG at 5 Hz.

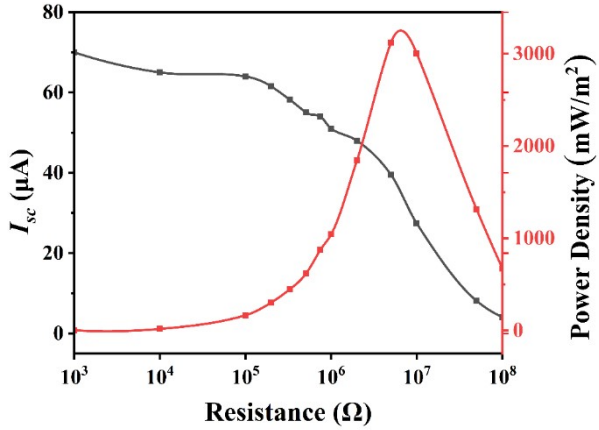

Figure S16. I_{sc} and power density of **2**-TEG under different external load resistance.

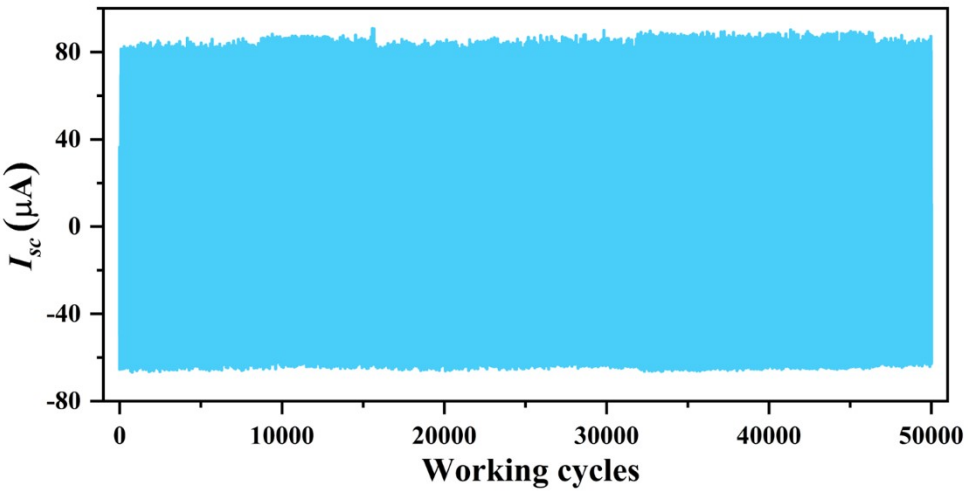

Figure S17. I_{sc} of **2**-TEG after working 50,000 cycles.

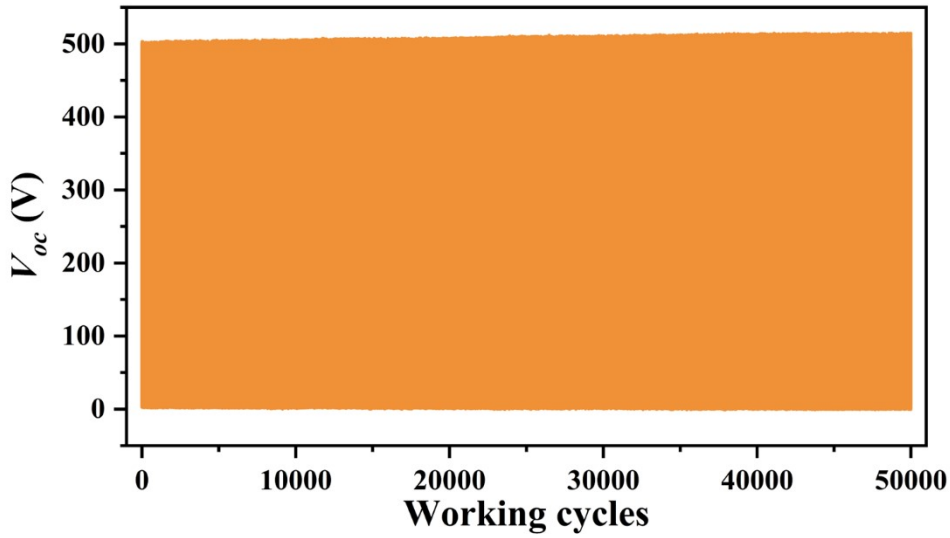

Figure S18. V_{oc} of **2**-TEG after working 50,000 cycles.

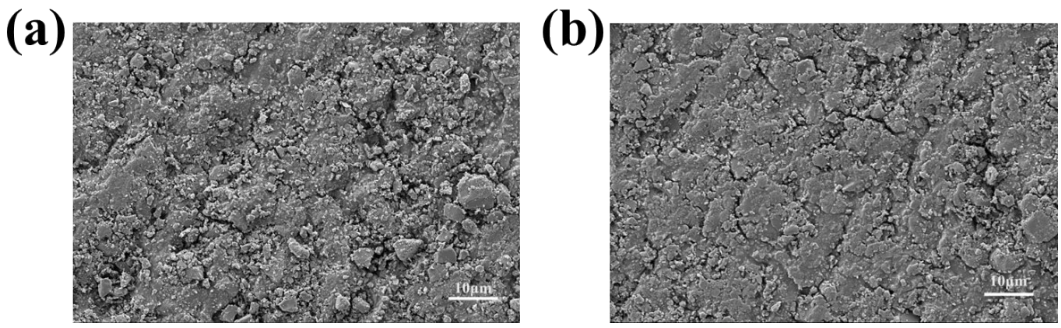

Figure S19. SEM image of samples of **2** on the Cu layer (a) before and (b) after collision.

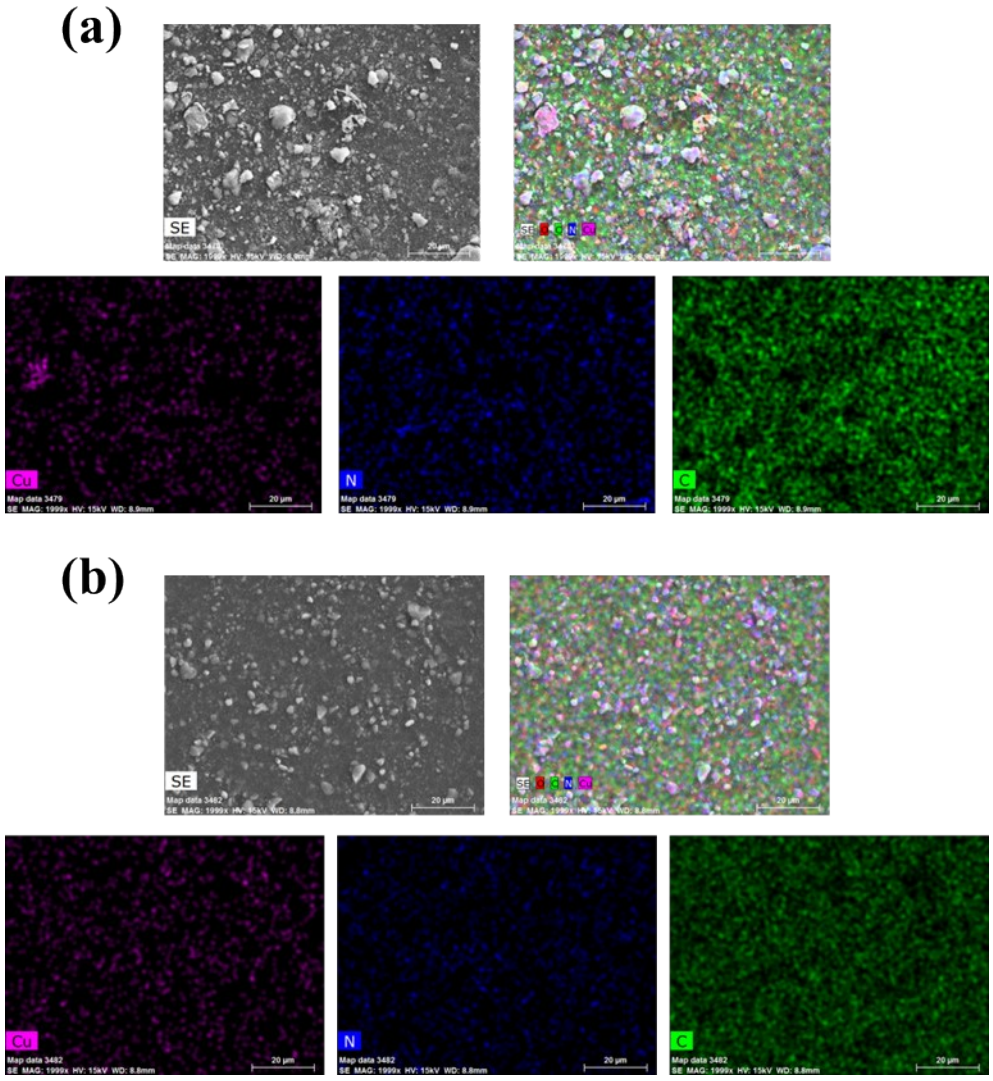

Figure S20. Elemental mapping images of **2** (a) before and (b) after measurement.

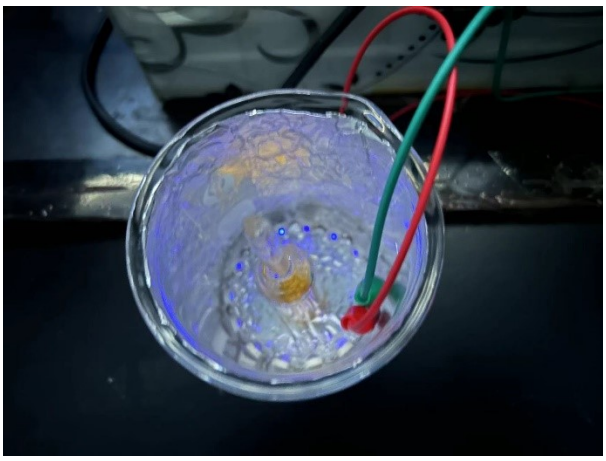

Figure S21. The digital photograph of 14 LED beads powered by the **2-TEG**.

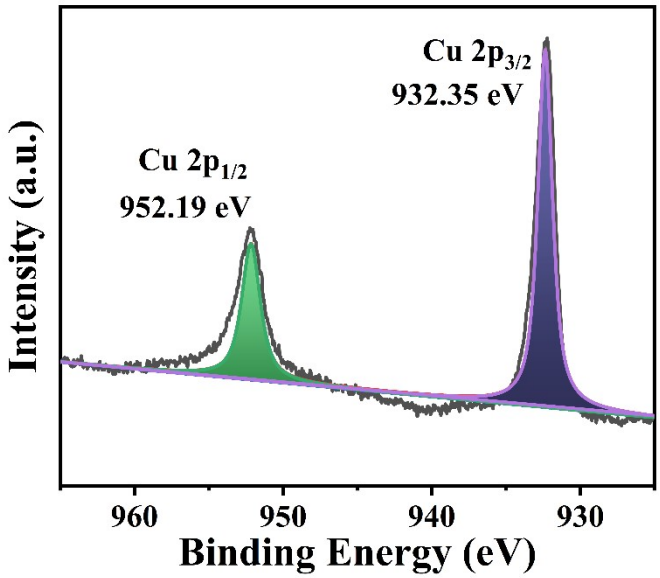

Figure S22. XPS spectra of **2** after photocatalytic C-H arylation reaction.

Table S4. Optimization of photocatalytic C-H arylation reactions using a **2**-TEG device [a].

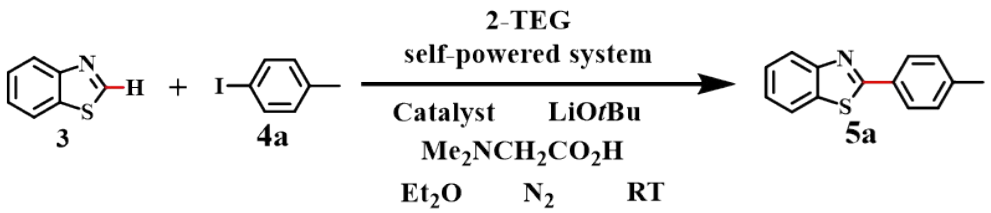

Entry	Catalysts (mol%)	Light	Time	Yield (%) [b]
1[c]	**CuI** (5)	+	4	53 %
2[c]	**1** (5)	+	4	32 %
3[c]	**2** (5)	+	4	65 %
4[d]	**CuI** (5)	+	4	67 %
5[d]	**1** (5)	+	4	40 %
6[d]	**2** (5)	+	4	74 %
7	**2** (10)	+	4	76 %
8	**2** (15)	+	4	79 %
9	**2** (20)	+	4	81 %
10	**2** (15)	+	6	83 %
11	**2** (15)	+	8	86 %
12	**2** (15)	+	10	90 %
13	**2** (15)	+	12	91 %
14	/[e]	+	10	0 %
15	**2** (15)	-[f]	10	0 %

[a]Benzothiazole (**3**, 0.5 mmol), aromatic iodides (**4a**, 2.5 mmol), catalyst (CuI/**1**/**2**, 15 mol %), $Me_2NCH_2CO_2H$ (30 mol %), LiO*t*Bu (1.5 mmol), and Et_2O (3 mL), 23-25 ℃ (temperature). [b] Yield of isolated product. [c] With the aid of organic ligand. [d] Without the aid of organic ligand. [e] Without the catalysts. [f] Without light.

7. Spectral copies of ^{1}H NMR of compounds obtained in this study

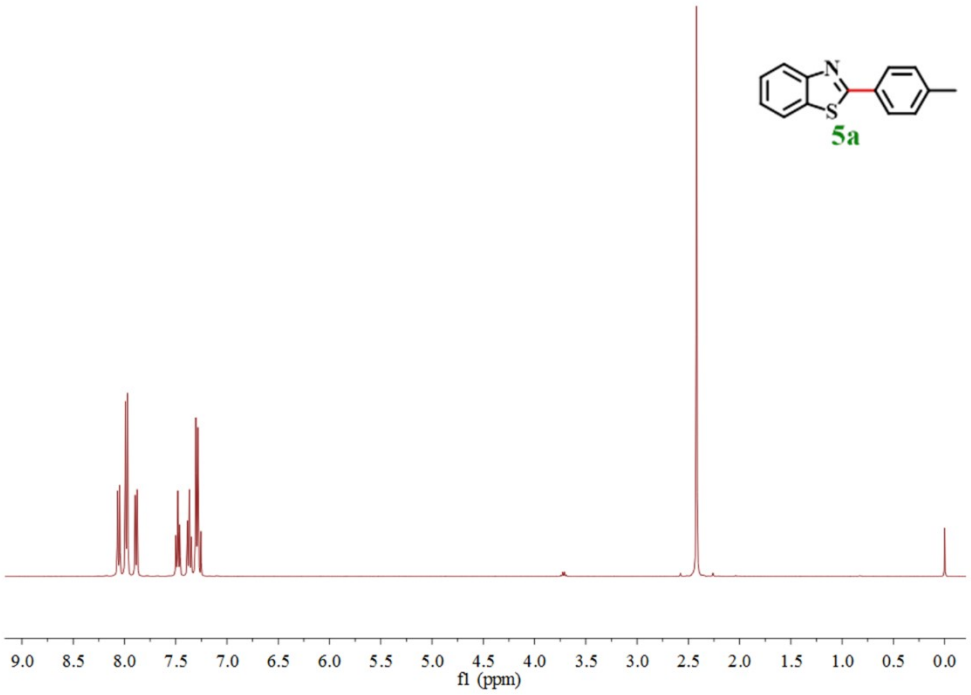

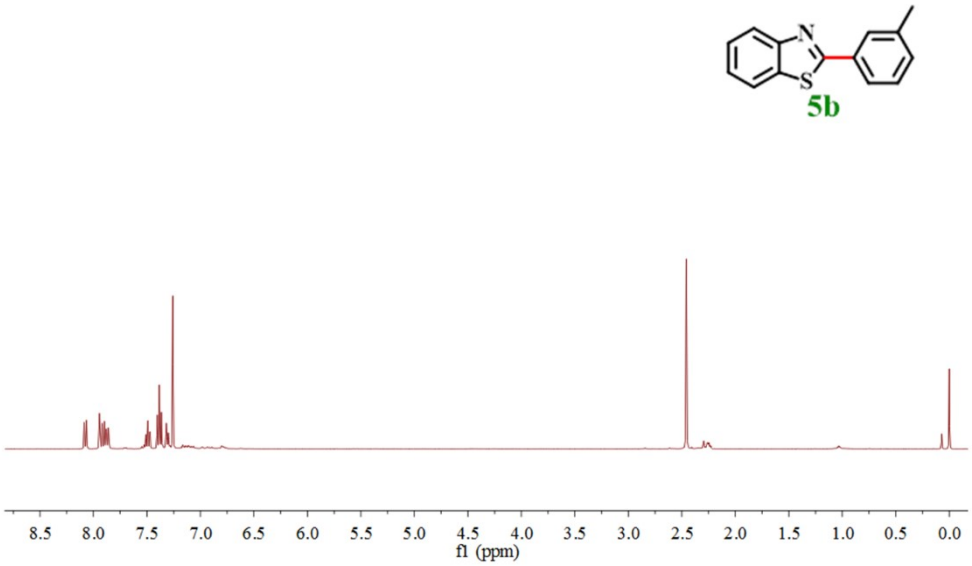

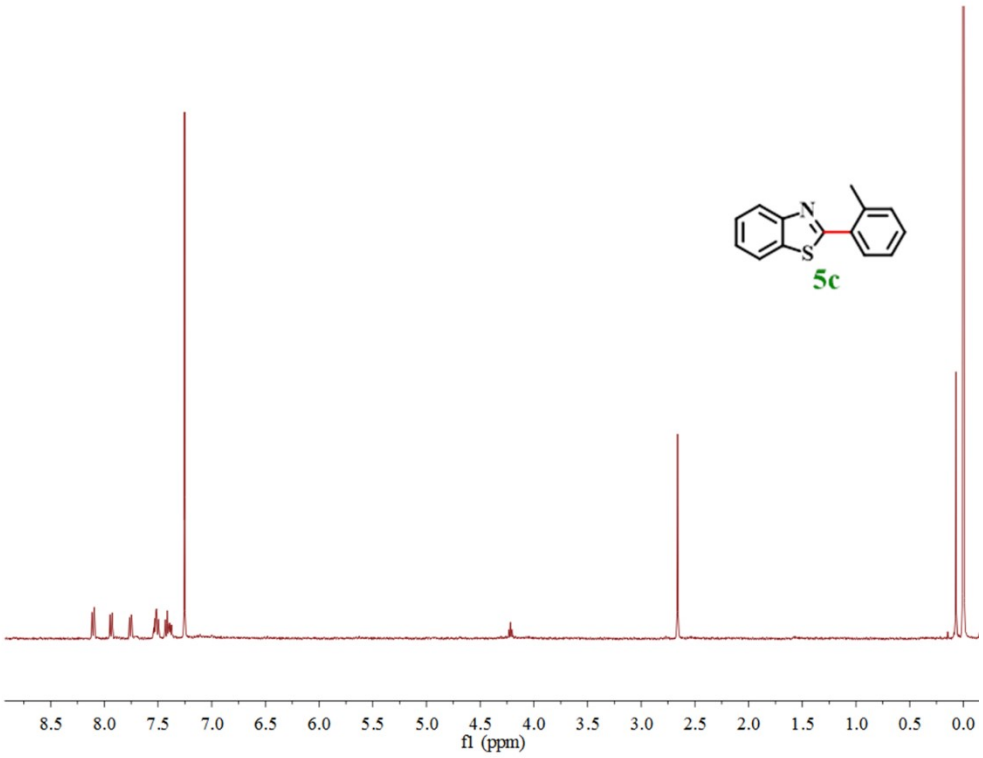
5c
8.5 8.0 7.5 7.0 6.5 6.0 5.5 5.0 4.5 4.0 3.5 3.0 2.5 2.0 1.5 1.0 0.5 0.0
f1 (ppm)

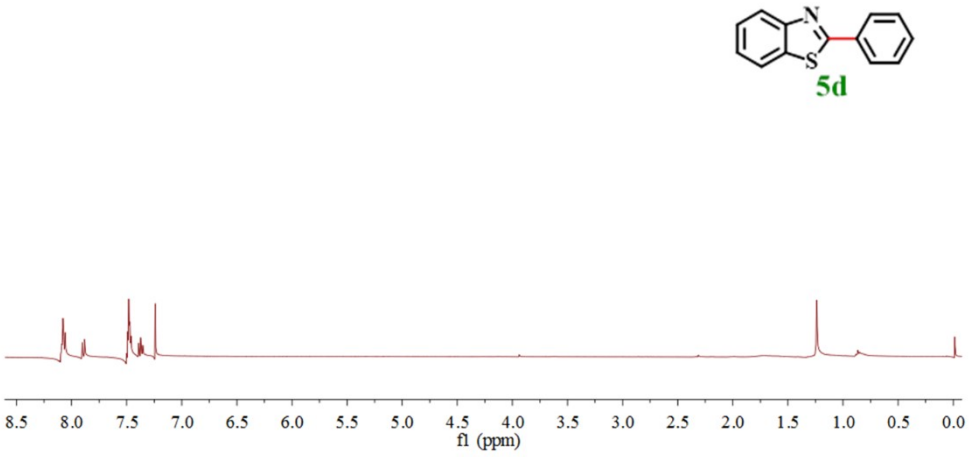
5d
8.5 8.0 7.5 7.0 6.5 6.0 5.5 5.0 4.5 4.0 3.5 3.0 2.5 2.0 1.5 1.0 0.5 0.0
f1 (ppm)

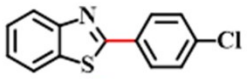
N
S
Cl

5e

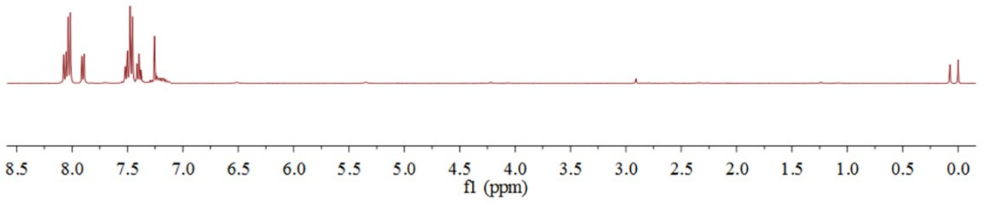
8.5 8.0 7.5 7.0 6.5 6.0 5.5 5.0 4.5 4.0 3.5 3.0 2.5 2.0 1.5 1.0 0.5 0.0
f1 (ppm)

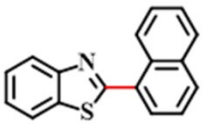
N
S

5f

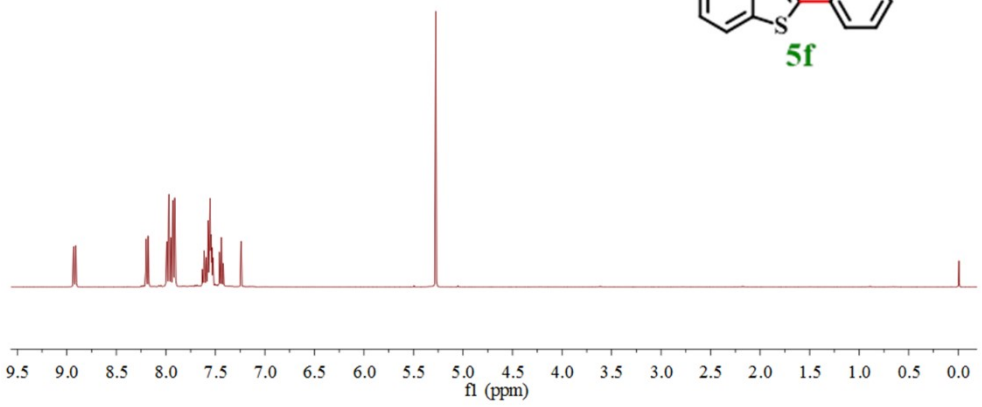
9.5 9.0 8.5 8.0 7.5 7.0 6.5 6.0 5.5 5.0 4.5 4.0 3.5 3.0 2.5 2.0 1.5 1.0 0.5 0.0
f1 (ppm)

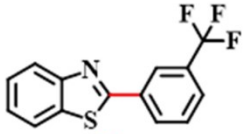
F
F
F
N
S

5g

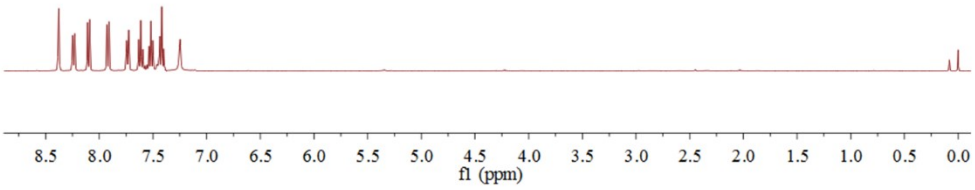
8.5 8.0 7.5 7.0 6.5 6.0 5.5 5.0 4.5 4.0 3.5 3.0 2.5 2.0 1.5 1.0 0.5 0.0
f1 (ppm)

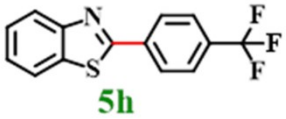
N
S
F
F
F

5h

8.5 8.0 7.5 7.0 6.5 6.0 5.5 5.0 4.5 4.0 3.5 3.0 2.5 2.0 1.5 1.0 0.5 0.0
f1 (ppm)

8. References

[1] (a) H. Lee, S. H. Jung, W. S. Han, J. H. Moon, S. Kang, J. Y. Lee, J. H. Jung and S. Shinkai, A Chromo-Fluorogenic Tetrazole-Based $CoBr_2$ Coordination Polymer Gel as a Highly Sensitive and Selective Chemosensor for Volatile Gases Containing Chloride, *Chem. Eur. J.* 2011, **17**, 2823-2827; (b) H. Lee, S. Kang, J. Y. Lee and J. H. Jung, Coordination polymer gel derived from a tetrazole ligand and Zn2+: spectroscopic and mechanical properties of an amorphous coordination polymer gel, *Soft Matter.* 2012, **8**, 2950-2955.

[2] S. Kori, Y. Bhujbal, K. Vadagaonkar, A. R. Kapdi, S. P. Kommyreddy and S. J. Gharpure, Room temperature HFIP/Ag-promoted palladium-catalyzed C-H functionalization of benzothiazole with iodoarenes, *Chem. Commun.* **2022**, 58, 847-850.

[3] F. Yang, J. Koeller and L. Ackermann, Photoinduced Copper-Catalyzed C-H Arylation at Room Temperature, *Angew. Chem., Int. Ed.* **2016**, 55, 4759-4762.

[4] G. Sheldrick, A short history of SHELX, *Acta Crystallogr., Sect. A: Found. Crystallogr.* 2007, **64**, 112-122.

[5] G. Sheldrick, Crystal structure refinement with SHELXL, *Acta Crystallogr., Sect. A: Found. Crystallogr.* 2015, **71**, 3-8.

[6] P. Zhu, Z. Ullah, S. Zheng, Z. Yang, S. Yu, S. Zhu, L. Liu, A. He, C. Wang and Q. Li, Ultrahigh current output from triboelectric nanogenerators based on UIO-66 materials for electrochemical cathodic protection, *Nano Energy*, 2023, **108**, 108195.

[7] G. Khandelwal, N. P. Maria Joseph Raj and S. J. Kim, Zeolitic Imidazole Framework: Metal-Organic Framework Subfamily Members for Triboelectric Nanogenerators, *Adv. Funct. Mater.*, 2020, **30**, 1910162.

[8] G. Khandelwal, A. Chandrasekhar, N. P. Maria Joseph Raj and S. J. Kim, Metal–Organic Framework: A Novel Material for Triboelectric Nanogenerator–Based Self-Powered Sensors and Systems, *Adv. Funct. Mater.*, 2019, **9**, 1803581.

[9] S. Barsiwal, A. Babu, U. K. Khanapuram, S. Potu, N. Madathil, R. K. Rajaboina, S. Mishra, H. Divi, P. Kodali, R. Nagapuri and T. Chinthakuntla, ZIF-67-Metal–Organic-Framework-Based Triboelectric Nanogenerator for Self-Powered Devices, *Nanoenergy Adv.*, 2022, **2**, 291-302.

[10] J. Swain, S. Hajra, N. Das, P. Parhi, S. Panda, A. Priyadarshini, J. Panda, A. K. Sahu, P. Alagarsamy, V. Vivekananthan, H. J. Kim and R. Sahu, Spent Catalyst-Derived Mo-MOF: Triboelectric Nanogenerators and Energy Harvesting, *Energy Technol.*, 2023, **11**, 2300498.

[11] K. Gao, J. Chen, M. Zhao, R. Hu, S. Chen, X. Xue, Z. Shao and H. Hou, 3D nanocrystalline metal–organic framework materials for the improved output performance of triboelectric nanogenerators, *Dalton Trans.*, 2023, **52**, 444-451.

[12] T. Wang, Q. Zhu, Q. Zhu, Q. Yang, S. Wang and L. Luo, A highly stable bimetallic organic framework for enhanced electrical performance of cellulose nanofiber-based triboelectric nanogenerators, *Nanoscale Adv.*, 2022, **4**, 4314-4320.

[13] Z. Chen, Y. Cao, W. Yang, L. An, H. Fan and Y. Guo, Embedding in-plane aligned MOF nanoflakes in silk fibroin for highly enhanced output performance of triboelectric nanogenerators, *J. Mater. Chem. A.*, 2022, **10**, 799-807.

[14] S. Hajra, M. Sahu, A. M. Padhan, I. S. Lee, D. K. Yi, P. Alagarsamy, S. S. Nanda and H. J. Kim, A Green Metal–Organic Framework-Cyclodextrin MOF: A Novel Multifunctional Material Based Triboelectric Nanogenerator for Highly Efficient Mechanical Energy Harvesting, *Adv. Funct. Mater.*, 2021, **31**, 210829.

[15] J. B. Xiong, Y. J. Zhou, S. H. Wang, Z. Q. Xiong, Z. K. Zhang, S. S. Zhang, C. K. Zhang, C. F. Xu and G. Q. Liu, Multi-F-Structured MOF Materials Enhance Nanogenerator Output Performance for Corrosion Protection of Metallic Materials, *Molecules*, 2023, **28**, 7894.